



HAL
open science

A method for multiple crack growth in brittle materials without remeshing

Elisa Budyn, Goangseup Zi, Nicolas Moës, Ted Belytschko

► **To cite this version:**

Elisa Budyn, Goangseup Zi, Nicolas Moës, Ted Belytschko. A method for multiple crack growth in brittle materials without remeshing. *International Journal for Numerical Methods in Engineering*, 2004, 61 (10), pp.1741-1770. 10.1002/nme.1130 . hal-01004845

HAL Id: hal-01004845

<https://hal.science/hal-01004845>

Submitted on 22 Jan 2023

HAL is a multi-disciplinary open access archive for the deposit and dissemination of scientific research documents, whether they are published or not. The documents may come from teaching and research institutions in France or abroad, or from public or private research centers.

L'archive ouverte pluridisciplinaire **HAL**, est destinée au dépôt et à la diffusion de documents scientifiques de niveau recherche, publiés ou non, émanant des établissements d'enseignement et de recherche français ou étrangers, des laboratoires publics ou privés.



Distributed under a Creative Commons Attribution - NonCommercial 4.0 International License

A method for multiple crack growth in brittle materials without remeshing

É. Budyn^{‡, ††}, G. Zi^{§, ¶}, N. Moës^{||, **} and T. Belytschko^{*, †, ‡‡}

*Department of Mechanical Engineering, Northwestern University, 2145 Sheridan Road,
Evanston, IL 60208, U.S.A.*

A method for modelling the growth of multiple cracks in linear elastic media is presented. Both homogeneous and inhomogeneous materials are considered. The method uses the extended finite element method for arbitrary discontinuities and does not require remeshing as the cracks grow; the method also treats the junction of cracks. The crack geometries are arbitrary with respect to the mesh and are described by vector level sets. The overall response of the structure is obtained until complete failure. A stability analysis of competitive cracks tips is performed. The method is applied to bodies in plane strain or plane stress and to unit cells with 2–10 growing cracks (although the method does not limit the number of cracks). It is shown to be efficient and accurate for crack coalescence and percolation problems.

KEY WORDS: multiple cracks; fracture; finite elements; stability; brittle material; junction; coalescence; percolation; unit cells; second variation of the energy

1. INTRODUCTION

We describe a method for modelling the evolution of multiple cracks in the framework of the eXtended Finite Element Method (X-FEM), which is a numerical method for treating arbitrary

*Correspondence to: T. Belytschko, Department of Mechanical Engineering, Northwestern University, 2145 Sheridan Road, Evanston, IL 60208, U.S.A.

†E-mail: tedbelytschko@northwestern.edu

‡Post-doctoral Research Fellow.

§E-mail: g-zi@korea.ac.kr

¶Assistant Professor

||E-mail: nicolas.moes@ec-nantes.fr

**Professor, Ecole Centrale Nantes, 1 rue de la Noé, 44321 Nantes, France.

††E-mail: e-budyn@alumni.northwestern.edu

‡‡Walter P. Murphy Professor of Mechanical Engineering.

Contract/grant sponsor: Office of Naval Research

Contract/grant sponsor: Department of Energy

discontinuities without remeshing [1, 2]. The discontinuities are represented by enriching the standard finite element approximation space. For cracks, suitable enrichments are the Heaviside function for the crack and the Westergaard field for the crack tip. X-FEM is an application of the partition of unity [3] and was introduced in References [1, 4, 5].

The crack topology is represented by vector level sets. Level sets were developed by Osher and Sethian [6, 7] for problems of interface tracking. Later Burchard *et al.* [8] and Osher *et al.* [9] considered the evolution of curves by level sets. Here we use a vector level set method developed by Ventura *et al.* [10, 11], because this method simplifies the process of freezing the existing level sets for cracks [2].

The mechanics of two interacting cracks in a brittle material has been studied in the experiments of Tanaka *et al.* [12], Lawler [13] and Barpi and Valente [14]. Analytic solutions for materials containing random distributions of cracks, such as Poisson distributions, were reported by Datsyshin and Savruk [15], Kachanov [16–18], Rubinstein [19–21], and Freji-Ayoub *et al.* [22]. Dyskin *et al.* [23] developed singular integral equations methods for random and regular distributions of cracks. Stochastic methods were developed by Bolotin [24], Yang *et al.* [25], Lua *et al.* [26–28] and McDonald [29]. Fractal methods for multiple crack problems were studied by Rybaczuk and Stoppel [30]. Boundary elements were applied to multiple crack problem by Carpinteri and Monetto [31].

We present a finite element method for multiple crack growth in a continuum. The method is applied in the context of linear fracture mechanics and is implemented with the extended finite element method. It does not require remeshing as the cracks grow. The cracks are grown until they coalesce and eventually percolate through the specimen. The model predicts final configurations that resemble experimental results for specimens containing random multiple cracks [13].

The cracks with the maximum stress intensity factors are grown so that they remain approximately at the critical stress intensity factor by adjusting the load parameter and solving for the corresponding displacement. The solution method is parametrized by crack length control. In the case of competing crack tips, a stability analysis is performed to determine the crack configuration path that leads to the maximum decrease in the potential energy. For junctions of cracks, a method is developed to handle crack tips impinging on existing cracks. Stress intensity factors are computed by means of an interaction integral [32].

The outline of this paper is as follows. The governing equations and the brittle fracture model are presented in Section 2. The finite element method for multiple crack problems and coalescence of cracks and percolation is presented in Section 3. In Section 4, the method for multiple crack growth in the framework of crack length control is given. A flowchart summarizes the method. Section 5 presents the results and studies the accuracy of the features developed for multiple crack problems. Conclusions are given in Section 6.

2. DESCRIPTION OF THE PROBLEM

We consider a two-dimensional elastic body Ω with boundary Γ , n_c cracks with surfaces $\Gamma_{cr} = \{\Gamma_{cr}^\alpha, \alpha = 1 \text{ to } n_c\}$, and n_t crack tips as shown in Figure 1. The normal to a surface is denoted by \mathbf{n} . The cracks are assumed to be traction free. Prescribed tractions \mathbf{t} are imposed on the boundary Γ_t and prescribed displacements are imposed on Γ_u . The implementation is limited to linear elastic fracture mechanics. The equilibrium equation and boundary conditions

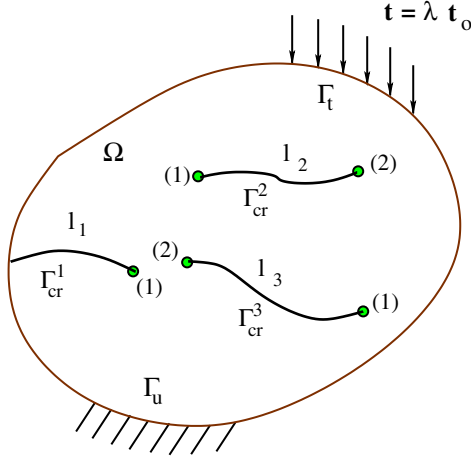


Figure 1. Description of a body containing multiple cracks.

are given by:

$$\nabla \cdot \boldsymbol{\sigma} = \mathbf{0} \quad \text{in } \Omega \quad (1)$$

$$\boldsymbol{\sigma} \cdot \mathbf{n} = \mathbf{t} \quad \text{on } \Gamma_t \quad (2)$$

$$\mathbf{u} = \bar{\mathbf{u}} \quad \text{on } \Gamma_u \quad (3)$$

where $\boldsymbol{\sigma}$ is the stress, $\mathbf{u}(\mathbf{x})$ is the displacement field, $\mathbf{u}^T = \{u_x, u_y\}$; $\bar{\mathbf{u}}$ is the prescribed displacement on Γ_u .

The stress–strain law is:

$$\boldsymbol{\sigma} = \mathbf{C} : \boldsymbol{\varepsilon} \quad (4)$$

where \mathbf{C} is the tensor of elastic moduli, and $\boldsymbol{\varepsilon}$ is the strain, given by:

$$\boldsymbol{\varepsilon} = \frac{1}{2}(\nabla \mathbf{u} + (\nabla \mathbf{u})^T) \quad (5)$$

The superscript T denotes the transpose of the matrix. We denote the length of each crack by l_i ; we denote the set of crack lengths by a matrix $\boldsymbol{\ell} = \{l_i\}$, $i = 1$ to n_t . The imposed traction \mathbf{t} depends linearly on a scalar parameter called the load factor λ : $\mathbf{t} = \lambda \mathbf{t}_o$, where \mathbf{t}_o is a reference traction field.

A brittle body containing multiple cracks in linear fracture mechanics can be described by the following Lagrangian form:

$$\mathcal{L}(\boldsymbol{\ell}, \mathbf{u}) = \mathcal{W}(\boldsymbol{\ell}, \mathbf{u}) + \sum_{i=1}^{n_t} \int_{\Gamma_{cr}^i} G_c^i dl_i \quad (6)$$

where $\mathcal{W}(\boldsymbol{\ell}, \mathbf{u})$ is the potential energy of the system, G_c^i is the critical energy release rate at crack tip i . In a homogeneous material, G_c is constant in the body, but for a heterogeneous

material G_c can be a function of (x, y) . If we define n_{act} as the number of active crack tips, the second term in the right-hand side of Equation (6) is the energy dissipated during the growth of the n_{act} active crack tips. The potential energy $\mathcal{W}(\ell, \mathbf{u})$ can be decomposed into the strain energy \mathcal{W}^{int} and the load potential \mathcal{W}^{ext} :

$$\mathcal{W}(\ell, \mathbf{u}) = \mathcal{W}^{\text{int}}(\ell, \mathbf{u}) - \mathcal{W}^{\text{ext}}(\mathbf{u}) \quad (7)$$

where

$$\mathcal{W}^{\text{int}}(\ell, \mathbf{u}) = \frac{1}{2} \int_{\Omega \setminus \Gamma_{\text{cr}}} \boldsymbol{\varepsilon}(\ell, \mathbf{u}) : \mathbf{C} : \boldsymbol{\varepsilon}(\ell, \mathbf{u}) \, d\Omega \quad (8)$$

$$\mathcal{W}^{\text{ext}}(\mathbf{u}) = \lambda \int_{\Gamma_i} \mathbf{t}_o \cdot \mathbf{u} \, d\Gamma \quad (9)$$

The equilibrium states of the body Ω correspond to the stationary points of (6) or points on the boundary of the feasible domain, so the solution $\mathbf{u} \in \mathcal{U}$ corresponds to:

$$\delta \mathcal{L} = \delta_{\mathbf{u}} \mathcal{W}(\ell, \mathbf{u}) \delta \mathbf{u} + \sum_{i=1}^{n_i} \left[\frac{\partial \mathcal{W}(\ell, \mathbf{u})}{\partial \ell_i} + G_c^i \right] \delta \ell_i \geq 0 \quad \forall \delta \mathbf{u} \in \mathcal{U}_o \quad \forall \delta \ell_i > 0 \quad (10)$$

where $\delta_{\mathbf{u}} \mathcal{W}(\ell, \mathbf{u})$ is the variation of \mathcal{W} with respect to \mathbf{u} , $\delta \mathbf{u}$ is the variation of the displacement and $d\ell_i$ is a crack length differential and:

$$\mathcal{U} = \{ \mathbf{u} / \mathbf{u} \in \mathcal{H}^1(\Omega \setminus \Gamma_{\text{cr}}), \llbracket \mathbf{u} \cdot \bar{\mathbf{n}} \rrbracket \geq 0 \text{ on } \Gamma_{\text{cr}}^\alpha, \mathbf{u} = \bar{\mathbf{u}} \text{ on } \Gamma_u \} \quad (11)$$

$$\mathcal{U}_o = \mathcal{U} \cap \{ \mathbf{u} / \mathbf{u} = 0 \text{ on } \Gamma_u \} \quad (12)$$

where $\bar{\mathbf{n}}$ is the normal to the crack and \mathcal{H}^1 is the Hilbert space of functions with square integrable derivatives. Note that the displacement field is discontinuous across the crack and that the jump $\llbracket \cdot \rrbracket$ in the normal displacement is required to be non-negative.

The above gives:

$$\delta_{\mathbf{u}} \mathcal{W}(\ell, \mathbf{u}) = 0 \quad (13)$$

$$\frac{\partial \mathcal{W}(\ell, \mathbf{u})}{\partial \ell_i} + G_c^i = -G_i + G_c^i \geq 0 \quad \forall i \in \{1, \dots, n_i\} \quad (14)$$

where we have used

$$G_i = - \frac{\partial \mathcal{W}(\ell, \mathbf{u})}{\partial \ell_i} \quad (15)$$

and (13) is the equilibrium equation and (14) is the Griffith criterion for each crack tip i . G_i is the energy release rate at tip i .

The crack growth law (14) can also be expressed in terms of stress intensity factors. The stress intensity factor at tip i , K_i , can be obtained from the energy release rate by:

$$K_i = \sqrt{E' G_i} \quad (16)$$

where E' is the effective Young's modulus (E' is equal to E in plane stress and $E/(1 - \nu^2)$ for plane strain). Therefore the critical stress intensity factor at tip i is $K_c^i = \sqrt{E'G_c^i}$.

The equivalent stress intensity factor at tip i , K_{eq}^i , can also be obtained from the interaction integrals in mode I and mode II [33, 1]:

$$K_{\text{I}}^i = \frac{E' I_{\text{I}}^i}{2} \quad (17)$$

$$K_{\text{II}}^i = \frac{E' I_{\text{II}}^i}{2} \quad (18)$$

where I_{I}^i and I_{II}^i , respectively, represent the interaction integral in mode I and II at tip i . The equivalent stress intensity factor is computed by [34]:

$$K_{\text{eq}}^i = \sqrt{(K_{\text{I}}^i)^2 + (K_{\text{II}}^i)^2} \simeq K_i \quad (19)$$

The crack growth law in linear elastic fracture mechanics of Equation (14) can also be written as:

$$\begin{aligned} \text{if } 0 < K_{\text{eq}}^i < K_c^i \quad \Delta \ell_i = 0 \quad (\text{no growth}) \\ \text{if } K_{\text{eq}}^i = K_c^i \quad \Delta \ell_i \geq 0 \quad (\text{growth}) \end{aligned} \quad (20)$$

where $\Delta \ell_i$ is the crack growth increment of tip i . We do not consider any closure of the cracks, though we note that $\Delta \ell_i < 0$ is not a valid solution. If the crack closes, the inequality $[[\mathbf{u} \cdot \bar{\mathbf{n}}]] \geq 0$ must be enforced.

The cracks are grown in the direction of the maximum hoop stress, θ^i . The angle θ^i is computed relative to the tangent to the crack tip at step $n - 1$, using the stress intensity factors at step $n - 1$ by:

$$\theta^i = 2 \arctan \left(\frac{1}{4} \left(K_{\text{I}}^i / K_{\text{II}}^i \pm \sqrt{(K_{\text{I}}^i / K_{\text{II}}^i)^2 + 8} \right) \right) \quad (21)$$

The above gives two directions; we choose the angle that corresponds to the positive maximum hoop stress.

The stress intensity factors K_{I}^i and K_{II}^i are computed by an interaction integral. The equivalent stress intensity factor is computed by (19). The expressions for the J -integral and the interaction integral as domain integrals can be found in Reference [32]. The multiple crack problem requires a stability analysis to determine the configuration path of crack evolution that is most stable, detailed in Section 4.

3. DISCRETIZATION

3.1. X-FEM formulation

The approximate displacement field is constructed by the extended finite element method (X-FEM). Two types of enrichments are needed to represent a crack: a step function for the

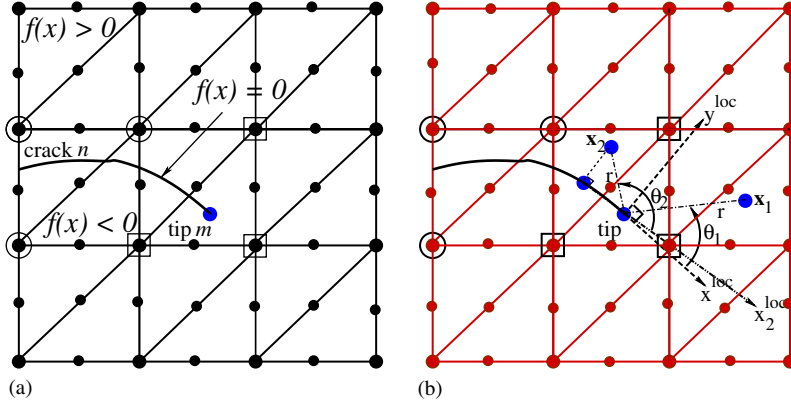


Figure 2. X-FEM representation of a crack. The circled nodes are enriched by the step function of crack n and the square nodes are enriched with the tip enrichment of tip m . The function f gives the distance of a point to the crack.

discontinuity of the interior of a crack and the asymptotic near-tip displacement field at the tips of the cracks [1, 5]. Figure 2 illustrates the enrichment scheme: all nodes of elements cut by a crack are enriched by the step function, and the nodes of the elements containing a crack tip are enriched by the near-tip displacement field.

Consider a mesh with a set of nodes \mathcal{I} . All corner nodes of elements crossed by a crack will be enriched. Let the set \mathcal{J}^n be the set of corner nodes of the elements cut by the crack n . The nodes of \mathcal{J}^n are enriched by the step function of crack n (circled nodes in Figure 2). Let \mathcal{K}^m be the set of corner nodes of the element that contains the crack tip m . These nodes are enriched by the branch function (squared nodes in Figure 2). We denote by \mathcal{N}_c the set of cracks and by \mathcal{N}_t the set of crack tips in the entire model. The crack geometry of crack n is described by the signed distance function $f^n(\mathbf{x})$ through:

$$f^n(\mathbf{x}) = 0 \quad (22)$$

For each crack the positions of the crack tips must be also specified. The signed distance function is updated by the vector level set method as in Reference [11].

The displacement field is based on Reference [35] adapted for multiple crack problems and is given by:

$$\mathbf{u}^h(\mathbf{x}) = \sum_{I \in \mathcal{I}} N_I(\mathbf{x}) u_I + \sum_{n=1}^{n_c} \sum_{J \in \mathcal{J}^n} \tilde{N}_J(\mathbf{x}) a_J^n \tilde{H}_J^n(\mathbf{x}) + \sum_{m=1}^{n_t} \sum_{K \in \mathcal{K}^m} \tilde{N}_K(\mathbf{x}) \left(\sum_{l=1}^4 b_{lK}^m \bar{F}_{lK}^m(\mathbf{x}) \right) \quad (23)$$

where $N_I(\mathbf{x})$ are the shape functions for the continuous displacement field; $\tilde{N}_J(\mathbf{x})$ are the shape functions applied to the enrichment field. This choice of shape functions for the enrichment field is explained in References [35, 36]. a_J^n are the additional unknowns for the modified step enrichment $\tilde{H}_J^n(\mathbf{x})$ of crack n and b_{lK}^m are the additional unknowns for the tip enrichment of tip m for the modified l th branch function $\bar{F}_{lK}^m(\mathbf{x})$; and \mathbf{x}_J is the position of node J . The

modified enrichment functions \bar{H}_J^n and \bar{F}_{lK}^m are given by:

$$\bar{H}_J^n(\mathbf{x}) = H(f^n(\mathbf{x})) - H(f^n(\mathbf{x}_J)) \quad (24)$$

$$\bar{F}_{lK}^m(\mathbf{x}) = F_l^m(\mathbf{x}) - F_l^m(\mathbf{x}_K) \quad (25)$$

and the step function H is given by:

$$H(x) = \begin{cases} +1 & \text{for } x > 0 \\ -1 & \text{for } x < 0 \end{cases} \quad (26)$$

The asymptotic neartip field is represented by a set of four functions F_l , as introduced by Fleming *et al.* [37]:

$$\{F_l(r, \theta)\}_{l=1,2,3,4} = \left\{ \sqrt{r} \sin \frac{\theta}{2}, \sqrt{r} \cos \frac{\theta}{2}, \sqrt{r} \sin \frac{\theta}{2} \sin \theta, \sqrt{r} \cos \frac{\theta}{2} \sin \theta \right\} \quad (27)$$

where r is a polar radius in a local co-ordinate system centred on the crack tip $(x^{\text{loc}}, y^{\text{loc}})$, i.e. $r = \|\mathbf{x} - \mathbf{x}^{\text{tip}}\|$, as shown in Figure 2. The x^{loc} -axis is aligned tangent to the crack at its tip and points away from the crack. The y^{loc} -axis is perpendicular to the x^{loc} -axis and follows the right-hand rule. To take into account any curvature of the crack, θ depends on \mathbf{x} . At a point beyond the crack tip (where $x^{\text{loc}} \geq 0$), θ is taken as the regular polar angle in the local reference axis system centred on the crack tip, as shown in Figure 2 for point \mathbf{x}_1 . For any point with $x^{\text{loc}} \leq 0$, for instance point \mathbf{x}_2 in Figure 2, θ is computed to reflect the curvature of the crack by (see Reference [2]):

$$\arctan(\theta) = \frac{f}{-\sqrt{r^2 - f^2}} \quad (28)$$

The minus sign in the above in the arctan argument is needed to reconcile this definition with the regular polar co-ordinates. For a crack with two tips, one must be careful with the sign of f , which should be reversed at the second tip of the crack to be consistent with the local polar orientation (where the sign of f is the negative value of y^{loc}).

The displacement field (23) allows the treatment of multiple cracks. The shape functions for the enrichment, \tilde{N}_J , differ from the shape functions for the standard displacement approximation N_J . In this work, the standard displacement shape functions are quadratic and the enrichment shape functions are linear. This choice smoothes the solution in the blending elements which are partially enriched in which the partition of unity does not hold. Applying linear shape functions to the branch enrichment introduces small errors in the blending element as explained in Reference [36] for other cases.

Note that the enrichment for each crack is local. For a step function enrichment, it does not extend beyond the elements that enclose the crack. For a branch function enrichment, it includes the element containing the crack and the immediately adjacent elements. Consequently, the size of the global stiffness matrix of the system is not much larger than that of the standard stiffness. Taking advantage of this requires that the additional unknowns be added in a linked list, so that the enrichment unknowns a_J^n and b_{lK}^m are mapped to a one-dimensional array. This aspect is important in multiple crack problems where many elements are enriched.

3.2. Discretization

The displacement approximation in (23) can be written as:

$$\mathbf{u}(\mathbf{x}) = \bar{\mathbf{N}}(\mathbf{x})\bar{\mathbf{d}} \quad (29)$$

where $\bar{\mathbf{N}}$ is the generalized shape function for the standard and enriched parts of the displacement field and the generalized nodal displacement matrix $\bar{\mathbf{d}}$ is:

$$\bar{\mathbf{d}}^T = [\mathbf{u}, \mathbf{a}, \mathbf{b}_1, \mathbf{b}_2, \mathbf{b}_3, \mathbf{b}_4] \quad (30)$$

where \mathbf{u} is the matrix of standard nodal displacements, \mathbf{a} are the unknowns for the step enrichment, and \mathbf{b}_l ($l = 1, 2, 3, 4$) are the unknowns for the branch enrichment.

The vector \mathbf{a} contains the additional degrees of freedom due to the step enrichment of all the cracks, and is written as:

$$\mathbf{a}^T = [\mathbf{a}^1, \dots, \mathbf{a}^n, \dots, \mathbf{a}^{n_c}] \quad \forall n \in \mathcal{N}_c \quad (31)$$

where \mathbf{a}^n is a vector that contains the extra degrees of freedom a_{xJ}^n and a_{yJ}^n of nodes $J \in \mathcal{J}^n$ due to the step enrichment of crack n .

In this paragraph, each vector \mathbf{b}_l or \mathbf{b}_l^m is denoted \mathbf{b} or \mathbf{b}^m to simplify the notation. The vector \mathbf{b} contains the additional degrees of freedom of the l th branch function due to the tip enrichment of all tips, and is written as:

$$\mathbf{b}^T = [\mathbf{b}^1, \dots, \mathbf{b}^m, \dots, \mathbf{b}^{n_t}] \quad \forall m \in \mathcal{N}_t, \quad l \in \{1, 2, 3, 4\} \quad (32)$$

where \mathbf{b}^m is a vector that contains of the extra degrees of freedom b_{xK}^m and b_{yK}^m of nodes $K \in \mathcal{K}^m$ due to the tip enrichment of tip m .

The discretized equilibrium equation (13) corresponds to the stationary points of the discrete Lagrangian (29):

$$\frac{\partial \mathcal{L}(\ell, \bar{\mathbf{d}})}{\partial \bar{\mathbf{d}}} = \mathbf{K}\bar{\mathbf{d}} - \lambda \mathbf{f}^{\text{ext}} = 0 \quad (33)$$

where the first term of Equation (33) is the internal force vector (product of the stiffness matrix and nodal displacements for the linear case) and the second term is the external force vector \mathbf{f}^{ext} given by:

$$\mathbf{f}^{\text{ext}} = \int_{\Gamma_t} \bar{\mathbf{N}} \mathbf{t}_o \, d\Gamma \quad (34)$$

where the prescribed traction $\mathbf{t}_o = \sigma_o \mathbf{n}$, with \mathbf{n} being the normal to the edge and σ_o a chosen scalar.

The stiffness matrix \mathbf{K} is given by:

$$\mathbf{K} = \int_{\Omega \setminus \Gamma_{\text{cr}}} \bar{\mathbf{B}}^T \mathbf{C} \bar{\mathbf{B}} \, d\Omega \quad (35)$$

The strain-displacement matrix of element e , denoted by $\bar{\mathbf{B}}_e$, is:

$$\bar{\mathbf{B}}_e = [\mathbf{B}_e^u \quad \mathbf{B}_e^a \quad \mathbf{B}_e^{b_1} \quad \mathbf{B}_e^{b_2} \quad \mathbf{B}_e^{b_3} \quad \mathbf{B}_e^{b_4}] \quad (36)$$

where the contribution of the standard displacement field is denoted by \mathbf{B}_e^u and is given by:

$$\mathbf{B}_e^u = \begin{bmatrix} (N_I(\mathbf{x}))_{,x} & 0 & \dots \\ 0 & (N_I(\mathbf{x}))_{,y} & \dots \\ (N_I(\mathbf{x}))_{,y} & (N_I(\mathbf{x}))_{,x} & \dots \end{bmatrix} \quad \forall I \in (s_e \cap \mathcal{J}) \quad (37)$$

where s_e is the set of nodes of element e . Note that each element matrix $\bar{\mathbf{B}}_e$ always contains \mathbf{B}_e^u , but the presence of \mathbf{B}_e^a or \mathbf{B}_e^{bl} depends on whether the element contains a crack or crack tip or contains one or more common nodes with an element that contains a crack or crack tip; in most elements, neither applies.

The matrix \mathbf{B}_e^a contains the contribution of the step enrichment to the strain-displacement matrix for all cracks in element e and is given by:

$$\mathbf{B}_e^a = [\dots \mathbf{B}_e^{a^n} \dots] \quad \forall n \in \mathcal{N}_c^e \quad (38)$$

The contribution to the element matrix \mathbf{B}_e^a of the nodes enriched with the step enrichment of each crack n is denoted $\mathbf{B}_e^{a^n}$ and gives:

$$\mathbf{B}_e^{a^n} = \begin{bmatrix} (\tilde{N}_J(\mathbf{x})\bar{H}_J^n(\mathbf{x}))_{,x} & 0 & \dots \\ 0 & (\tilde{N}_J(\mathbf{x})\bar{H}_J^n(\mathbf{x}))_{,y} & \dots \\ (\tilde{N}_J(\mathbf{x})\bar{H}_J^n(\mathbf{x}))_{,y} & (\tilde{N}_J(\mathbf{x})\bar{H}_J^n(\mathbf{x}))_{,x} & \dots \end{bmatrix} \quad \forall J \in \mathcal{J}_e^n \text{ and } \forall n \in \mathcal{N}_c^e \quad (39)$$

where \mathcal{J}_e^n is the set of nodes in element e that require the step enrichment of crack n . Let s_e^* be the set of nodes of element e that are enriched (the three corner nodes in our approach), $\mathcal{J}_e^n = s_e^* \cap \mathcal{J}^n$; \mathcal{N}_c^e is the set of cracks in element e and is included in \mathcal{N}_c . It is usually easier to determine the list of cracks \mathcal{N}_c^e in element e and successively compute $H(f^n)$ for all nodes in \mathcal{J}_e^n for each crack n in \mathcal{N}_c^e . Note that the domain of integration does not include the crack, so in evaluating (39) we obtain:

$$(\tilde{N}_J(\mathbf{x})\bar{H}_J^n(\mathbf{x}))_{,x} = (\tilde{N}_J(\mathbf{x}))_{,x}\bar{H}_J^n(\mathbf{x}) \quad (40)$$

$$(\tilde{N}_J(\mathbf{x})\bar{H}_J^n(\mathbf{x}))_{,y} = (\tilde{N}_J(\mathbf{x}))_{,y}\bar{H}_J^n(\mathbf{y}) \quad (41)$$

For the each branch enrichment \bar{F}_l , an element matrix \mathbf{B}_e^{bl} is constructed in the same manner as the \mathbf{B}_e^a by assembling the contribution of each tip m in \mathcal{N}_t^e , which is denoted $\mathbf{B}_e^{bl^m}$. The matrix $\mathbf{B}_e^{bl^m}$ is constructed for the set of nodes denoted \mathcal{K}_e^m in element e with tip m branch enrichment; $\mathcal{K}_e^m = s_e^* \cap \mathcal{K}^m$, where \mathcal{N}_t^e is the set of tips in element e .

3.3. Crack tip reaching a free boundary or another crack

Multi-crack algorithms must deal with several situations, such as the junction of cracks and growth to a boundary, that cannot be treated in detail without slowing the algorithm. We must developed some heuristics for these situations that are described next. In each step, crack tips that grow are determined by a stability analysis on crack tips whose stress intensity factors have nearly reached their critical value. Crack tips that are identified to grow are treated separately

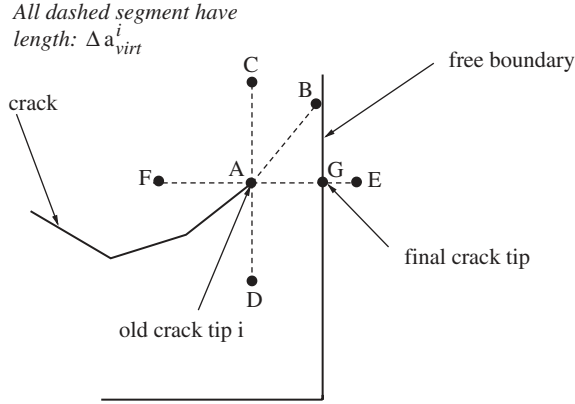


Figure 3. Tip of a crack approaching a free boundary.

if they reach a free boundary or another crack during a step. When this occurs, we annihilate or ‘kill’ the crack tip. When a crack tip joins with another crack, we introduce a ‘junction’ enrichment to account for the linked discontinuities.

For each crack tip i , consider a virtual increment $\Delta \ell_{\text{virt}}^i$. One possible approximation is to set $\Delta \ell_{\text{virt}}^i = \Delta \ell_{\text{tot}}$, where $\Delta \ell_{\text{tot}}$ is the total crack growth per step. A second more restrictive approach is to choose $\Delta \ell_{\text{virt}}^i = \max(\Delta \ell_i, r_i)$, where $\Delta \ell_i$ is the increment of growth of (44) and r_i is the radius of the domain of computation of the interaction integral at tip i ; the radius r_i is about twice the element length. In most cases, when the mesh is fine, we have found that when the elements of the annular domain on which the J -integral is computed are partially truncated by the boundary of the model or contains another crack, the stress intensity factors still gives the correct direction of propagation. However the second approach should be considered when many cracks interact.

3.3.1. Boundary algorithm. When the tip crosses the boundary, the branch function enrichment in Equation (23) is eliminated, i.e. ‘killed’, by setting $b_{lK}^m = 0$. Only the step function enrichment is retained. To determine where the crack intersects the free surface, the crack tip at the previous timestep, point A in Figure 3, is first extended by $\Delta \ell_{\text{virt}}^i$ in the direction of the maximum hoop stress, e.g. point B in Figure 3. If point B is outside the body, the final position of the tip is at the intersection between the free boundary and the virtual extension. If point B is inside the body, another test is performed by extending the crack by $\Delta \ell_{\text{virt}}^i$ in the direction normal to the nearest boundary, e.g. point E in Figure 3. If the latter point is outside the body, it is chosen as the crack path, and the final position of the tip is at the intersection G of the free boundary with the virtual extension of the crack $[AE]$ in Figure 3.

3.3.2. Coalescence detection algorithm. Most analytical methods assume ‘weak interactions’ (where cracks are quite far from each other) or ‘remotely located cracks’ (where cracks are very far from each other), i.e. Reference [16]. Multiple interacting cracks are difficult to model for many reasons. When two cracks approach each other the distribution of stresses changes rapidly and subsequently the material remaining between the cracks becomes very narrow [38].

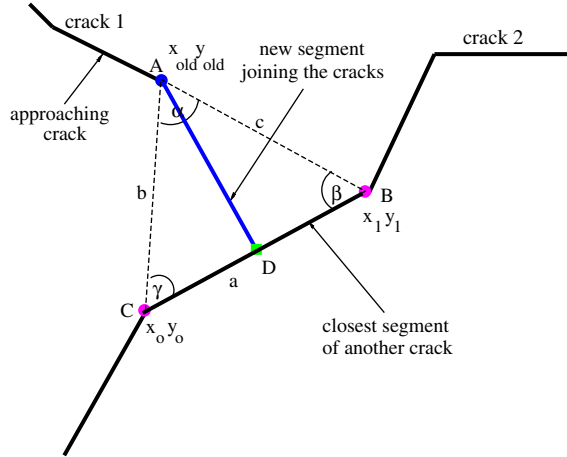


Figure 4. Junction of a crack with another crack.

Models such as local bond breaking within the remaining matrix may be appropriate. The notion of joining two interacting brittle cracks is based on the idea that a very small amount of brittle material subjected to a tensile stress will break and therefore the two cracks join. Bolander and Saito [39] studied the growth of multiple cracks by spring network methods. However, few experiments or numerical studies have been performed with distributions of growing cracks in a continuum.

The interactions of a major crack with an array of microcracks close to the tip has been studied in References [19, 20, 40–42]. Such approaches are relevant in the sense that a small ligament of material between two cracks in a brittle material degrades and leads to the junction of two neighbouring cracks.

In this work cracks are allowed to coalesce. The algorithm we choose for effecting the junction is similar to Reference [31]. We detect any impending intersection by finding the closest crack segment $[CB]$ from the tip of a crack at the previous step (x_{old}, y_{old}) , as in Figure 4. When the distance $[AD]$ between the growing crack tip (x_{old}, y_{old}) and the middle of the closest segment of another crack is less than the virtual crack length increment Δl_{virt} , the cracks are joined. The tip enrichment is removed from the element containing the joined cracks and only the step enrichment of both cracks is kept. A new step-junction enrichment is added as described in the next subsection.

In addition, a test is performed to avoid the creation of a rigid body mode. If two cracks are already connected to each other or connected to common cracks, we do not join the cracks, since this would render the stiffness matrix singular. One can consider the small ligament that is kept as a stabilizing mechanism for the equilibrium equations, which is probably valid as long as the loading is tensile. However we kill or deactivate the tip of the crack about to join the other one.

3.4. Junction approximation

In the framework of X-FEM, enrichments for crack junction have been developed by Daux *et al.* [43] and Belytschko *et al.* [2]. Here a similar but simpler method is developed. When two

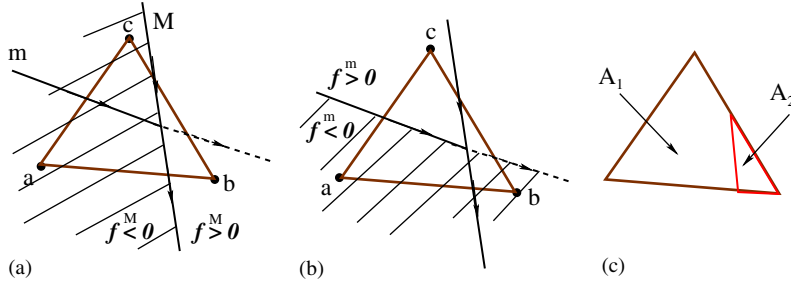


Figure 5. The signed distance functions of the ‘minor’ crack m and the ‘Master’ crack M . The ‘minor’ crack is the crack joining an existing crack, and the ‘Master’ crack is the crack that is being joined.

cracks intersect, the tip enrichment of the approaching crack is annihilated and is replaced by a Heaviside enrichment. In the element containing the junction of the two cracks, a Heaviside-junction enrichment $\bar{J}(\mathbf{x})$ models junction of the two cracks. We call the crack whose tip is killed (crack m in Figure 5) the minor crack and the other, the master crack (crack M in Figure 5). Let $f^m(\mathbf{x})$ be the signed distance function of the minor crack that joins the master crack given by the signed distance function $f^M(\mathbf{x})$, in Figure 5(a) and (b). The function $\bar{J}(\mathbf{x})$ models that the approaching crack m is arrested on the other crack M . When the two cracks have coalesced, the displacement field (23) in the element containing the junction is taken to be:

$$\mathbf{u}^e(\mathbf{x}) = \sum_{I \in \mathcal{I}_e} N_I(\mathbf{x}) u_I + \sum_{J \in \mathcal{J}_e^m} \tilde{N}_J(\mathbf{x}) a_J^m \bar{J}_J^m(\mathbf{x}) + \sum_{J \in \mathcal{J}_e^M} \tilde{N}_J(\mathbf{x}) a_J^M \bar{H}_J^M(\mathbf{x}) \quad (42)$$

where \bar{J} is the junction enrichment of crack m :

$$\bar{J}_J^m(\mathbf{x}) = \begin{cases} H(f^m(\mathbf{x})) - H(f^m(\mathbf{x}_J)) & \text{for } x \in A_1 \\ H(f^M(\mathbf{x})) - H(f^M(\mathbf{x}_J)) & \text{for } x \in A_2 \end{cases} \quad (43)$$

where A_2 is the side of the master crack that does not contain the minor crack. A_1 is the remaining area of the element that contains the junction.

3.5. Numerical integration of elements containing cracks

For accurate integration of the stiffness matrix and nodal forces, the elements containing discontinuities must be treated separately. Each element is subdivided into subtriangles obtained by Delaunay triangulation over the union of the corner nodes of the element, the intersection of the discontinuity with the edges of the element, and the crack tip locations as shown in Figure 6. In this example, five triangles are created. In each of these triangles, 13 point Gauss quadrature is used. The increase in computational cost is not significant as long as the number of enriched elements is much less than the number of non-enriched elements.

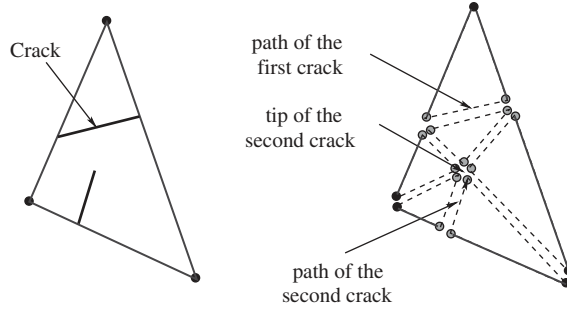


Figure 6. Delaunay partitioning of elements containing cracks.

4. SOLUTION ALGORITHM FOR MULTIPLE CRACK PROBLEM

In Section 3, the discretized equilibrium equation (33) was presented. This section describes an algorithm to satisfy both Equations (33) and (14). The discretized equilibrium (33) is solved for a prescribed traction \mathbf{t}_o and then the load parameter λ is adjusted to satisfy (14). The algorithm is explicit in that the crack growth increments are set at the beginning of each step and they are not adjusted. When a single crack grows, the crack growth law can be met exactly because the load parameter λ is adjusted so that the stress intensity factor of that crack remains at the critical value. When several cracks grow during a step, the explicit character of the algorithm results in the stress intensity factors of some growing cracks becoming less than critical.

4.1. Crack increment

The solution algorithm is based on a ‘crack length control’ scheme so that the evolution is controlled by a monotonically increasing function of the total crack length, i.e. the sum of all crack lengths [44]. It is able to capture the snap-back branch of the overall response of the structure. In each step the sum of crack increments is set equal to a fixed value $\Delta\ell_{\text{tot}}$. Within each step, the length of each active crack tip is increased in the direction of the maximum hoop stress by:

$$\Delta\ell_i = \frac{\Delta\ell_{\text{tot}}}{n_{\text{act}}} \quad (44)$$

where n_{act} is the number of active cracks that grow at the beginning of step n ; n_{act} is determined by a stability analysis at the end of step $n - 1$ to be described later. Note that $\Delta\ell_i$ is adjusted if the growing crack encounters a free boundary or another crack as explained in the previous section.

4.2. Calculation of the load parameter λ

At the beginning of each step n , we obtain the solution $\bar{\mathbf{d}}$ and the stress intensity factors for an applied traction \mathbf{t}_o . We then determine the tip β , which is the tip closest to its critical stress

intensity factor, i.e.:

$$\beta = \arg \left(\min_{i=1}^{n_t} \frac{K_c^i}{K_{\text{eq}}^i(\sigma_o)} \right) \quad (45)$$

For a homogeneous material where $K_c^i = K_c$ is constant over the body, β is the tip with the maximum equivalent stress intensity factor.

The load parameter λ is chosen so that the stress intensity factor of tip β attains the critical value K_c^β . Since the material is linear elastic, the parameter λ is given by:

$$\lambda = \frac{K_c^\beta}{K_{\text{eq}}^\beta(\sigma_o)} \quad (46)$$

In some cases, several cracks are close to the critical stress intensity factors. We call these crack tips the competitive crack tips and denote by $\mathcal{N}_{\text{comp}}$ the set of competitive crack tips. In other words, $\mathcal{N}_{\text{comp}}$ is the set of crack tips whose stress intensity factors $K_{\text{eq}}^i(\sigma_o)$ are close to their critical stress intensity factor K_c^i , i.e.:

$$\mathcal{N}_{\text{comp}} = \left\{ i \in \{1, \dots, n_t\} \text{ such that } \frac{\bar{\kappa}_\beta - \bar{\kappa}_i}{\bar{\kappa}_\beta} \leq \varepsilon \right\} \quad (47)$$

where $\bar{\kappa}_\beta = K_\beta(\sigma_o)/K_c^\beta$ and $\bar{\kappa}_i = K_i(\sigma_o)/K_c^i$. We set the tolerance ε to be about 1%. The active crack tips are then selected from the set of $\mathcal{N}_{\text{comp}}$ by the stability analysis described next.

4.3. Stability analysis and selection of active cracks

A stability analysis is conducted to determine the cracks that grow in a step. The most stable crack configuration evolution corresponds to that with the minimum energy dissipation. The stability of a crack configuration is examined by the second variation of the Lagrangian form (6). A crack configuration is stable if:

$$\frac{\partial^2 \mathcal{L}(\ell, \mathbf{u}(\ell))}{\partial \ell_i \partial \ell_j} > 0 \quad \forall i, j \in \{1, \dots, n_{\text{act}}\} \quad (48)$$

According to the definition of G_i in Equation (14), Equation (48) implies:

$$\left(\frac{\partial G_i}{\partial \ell_j} - \frac{\partial G_c^i}{\partial \ell_j} \right) < 0 \quad \forall i, j \in \{1, \dots, n_{\text{act}}\} \quad (49)$$

When several cracks are competing and there are several possible stable crack growth configuration paths, the most stable path is that which dissipates the least energy, and this is the one chosen. When the second variation of the Lagrangian form is negative, the path that causes the most damage to the structure is chosen.

To compute the derivatives of the energy release rate with respect to the crack length [45, 46], we use the expression developed by Suo and Combescure [47, 48] and Suo and Valeta [49], which is computed by a domain integral.

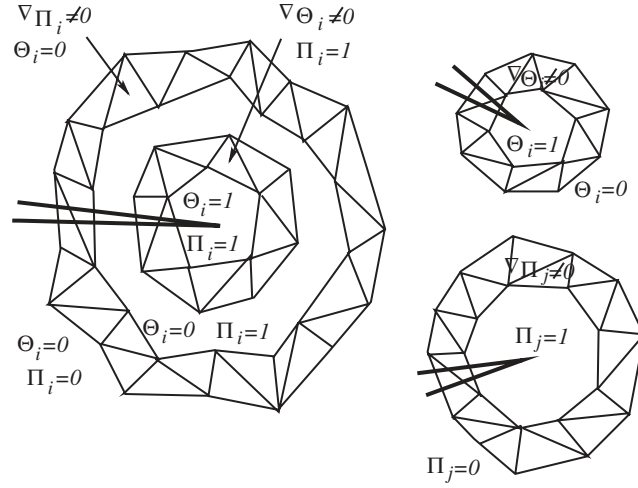


Figure 7. Virtual displacements at the tip of a crack for the calculation of the derivatives of the energy release rate. On the left-hand side are the virtual displacements for $\partial G_i / \partial \ell_j$ ($i = j$), and on the right-hand side are the virtual displacements for $\partial G_i / \partial \ell_j$ ($i \neq j$) [49].

From Equation (14), the derivative of the energy release rate at tip i with respect to tip j is given by:

$$\frac{\partial G_i}{\partial \ell_j} - \frac{\partial G_c^i}{\partial \ell_j} = -\frac{\partial^2 \mathcal{W}}{\partial \ell_i \partial \ell_j} - \frac{\partial G_c^i}{\partial \ell_j} \quad (50)$$

where \mathcal{W} is the potential energy of the system. The variation of crack length $\delta \ell_i$ will be obtained from a virtual displacement function $\Theta_i(\mathbf{x})$, and the virtual variation of crack length $\delta \ell_j$ will be obtained from a virtual displacement function $\Pi_j(\mathbf{x})$.

The region where the gradient of the functions Π_j and Θ_i are non-zero contains the elements in a circular region at the tip j and i , respectively, of a roughly annular shape as shown in Figure 7. In X-FEM, it is not necessary to move any of the nodes as in Reference [48]. The two functions Π_j and Θ_i are constructed as in Reference [49]. For ease of computation, we construct Π_j and Θ_i as combinations of constant functions and ramp functions that are parallel to the crack direction as shown in Figure 7.

As indicated in Figure 7, the domains where the gradients of Π_j and Θ_i are non-zero should not intersect when we compute the diagonal term of $[\partial G_i / \partial \ell_j]$; this is important as explained in Reference [47]. For this reason, the annular region where the gradient of Θ_i is non-zero must always be disjoint with the annular region where the gradient of Π_j is non-zero. For our calculation, the average radius of the region where the gradient of Θ_i is non-zero is about twice the element length, and the radius of the region where the gradient of Π_j is non-zero is about four times the element length. This ensures that the domains where the gradient of Θ_i and Π_j are non-zero are disjoint. The radius of the Θ_i domain of twice the element length also ensures that the annular domain where the gradient of Θ_i is non-zero does not include nodes with branch enrichment.

The computation of the derivative of the energy release rate $\partial G_i / \partial \ell_j$ requires the construction of a virtual displacement field $\tilde{\mathbf{d}}_j$ as explained in Reference [49]. The function Π_j is used to compute a virtual force field $\tilde{\mathbf{f}}_{\Pi_j}$ of the nodes around the tip j of a crack. In our calculation, the virtual displacement Π_j is a ramp function that is equal to 1 inside of the selected annular region, and vanishes outside the annular region and varies linearly from 1 to 0 in the annular region, see Figure 7. This virtual force $\tilde{\mathbf{f}}_{\Pi_j}$ is defined by:

$$\tilde{\mathbf{f}}_{\Pi_j} = \int_{\Omega \setminus \Gamma_{\text{cr}}} \bar{\mathbf{B}}^T (\mathbf{C} \tilde{\mathbf{B}}_{\Pi_j} \bar{\mathbf{d}} - \boldsymbol{\sigma} \text{div}(\Pi_j)) \, d\Omega + \int_{\Omega \setminus \Gamma_{\text{cr}}} \tilde{\mathbf{B}}_{\Pi_j}^T \boldsymbol{\sigma} \, d\Omega \quad (51)$$

where the matrix \mathbf{C} is the elastic constitutive matrix, the global matrix $\bar{\mathbf{B}}$ is defined in Section 3 and global matrix $\tilde{\mathbf{B}}_{\Pi_j}$ is constructed by assembling element matrices $\tilde{\mathbf{B}}_e$ that are functions of Π_j and defined by:

$$\tilde{\mathbf{B}}_e = [\tilde{\mathbf{B}}_e^u \quad \tilde{\mathbf{B}}_e^a \quad \tilde{\mathbf{B}}_e^{b1} \quad \tilde{\mathbf{B}}_e^{b2} \quad \tilde{\mathbf{B}}_e^{b3} \quad \tilde{\mathbf{B}}_e^{b4}] \quad (52)$$

The matrix $\tilde{\mathbf{B}}_e$ is assembled into $\tilde{\mathbf{B}}_{\Pi_j}$ in the same manner as the element B-matrix $\bar{\mathbf{B}}_e$ into $\bar{\mathbf{B}}$.

The contribution of the standard part of the displacement to the element matrix $\tilde{\mathbf{B}}_e$ is denoted $\tilde{\mathbf{B}}_e^u$ and has the following form:

$$\tilde{\mathbf{B}}_e^u = \begin{bmatrix} \mathcal{B}_{1I} & 0 & \dots \\ 0 & \mathcal{B}_{2I} & \dots \\ \mathcal{B}_{2I} & \mathcal{B}_{1I} & \dots \end{bmatrix} \quad \forall I \in (s_e \cap \mathcal{I}) \quad (53)$$

The terms \mathcal{B}_{1I} and \mathcal{B}_{2I} are defined by (see Reference [49]):

$$\mathcal{B}_{1I} = \frac{\partial N_I(\mathbf{x})}{\partial x} \frac{\partial \Pi_x^j}{\partial x} + \frac{\partial N_I(\mathbf{x})}{\partial y} \frac{\partial \Pi_y^j}{\partial x} \quad (54)$$

$$\mathcal{B}_{2I} = \frac{\partial N_I(\mathbf{x})}{\partial x} \frac{\partial \Pi_x^j}{\partial y} + \frac{\partial N_I(\mathbf{x})}{\partial y} \frac{\partial \Pi_y^j}{\partial y} \quad (55)$$

The element matrix $\tilde{\mathbf{B}}_e^a$ containing the contribution of the step enrichment of all cracks in element e , is then:

$$\tilde{\mathbf{B}}_e^a = [\dots \tilde{\mathbf{B}}_e^{a^n} \dots] \quad \forall n \in \mathcal{N}_c^e \quad (56)$$

The contribution of the step enrichment of each crack n to the element matrix $\tilde{\mathbf{B}}_e^a$ is denoted $\tilde{\mathbf{B}}_e^{a^n}$ and is as follows:

$$\tilde{\mathbf{B}}_e^{a^n} = \begin{bmatrix} \mathcal{B}_{1J}^{a^n} & 0 & \dots \\ 0 & \mathcal{B}_{2J}^{a^n} & \dots \\ \mathcal{B}_{2J}^{a^n} & \mathcal{B}_{1J}^{a^n} & \dots \end{bmatrix} \quad \forall J \in \mathcal{J}_e^n \text{ and } \forall n \in \mathcal{N}_c^e \quad (57)$$

The terms $\mathcal{B}_{1J}^{a^n}$ and $\mathcal{B}_{2J}^{a^n}$ are defined by:

$$\mathcal{B}_{1J}^{a^n} = \frac{\partial(\tilde{N}_J(\mathbf{x})\tilde{H}_J^n(\mathbf{x}))}{\partial x} \frac{\partial \Pi_x^j}{\partial x} + \frac{\partial(\tilde{N}_J(\mathbf{x})\tilde{H}_J^n(\mathbf{x}))}{\partial y} \frac{\partial \Pi_y^j}{\partial x} \quad (58)$$

$$\mathcal{B}_{2J}^{a^n} = \frac{\partial(\tilde{N}_J(\mathbf{x})\tilde{H}_J^n(\mathbf{x}))}{\partial x} \frac{\partial \Pi_x^j}{\partial y} + \frac{\partial(\tilde{N}_J(\mathbf{x})\tilde{H}_J^n(\mathbf{x}))}{\partial y} \frac{\partial \Pi_y^j}{\partial y} \quad (59)$$

In this paragraph, we describe the contribution of each branch enrichment \tilde{F}_l to $\tilde{\mathbf{B}}_e$. For simplicity of the expression we drop the l index and write b or b^m instead of b_l or b_l^m , $l = \{1, 2, 3, 4\}$. The elemental matrix $\tilde{\mathbf{B}}_e^b$ containing the contribution of the l th branch enrichment of all the tips present in element e , is then:

$$\tilde{\mathbf{B}}_e^b = [\dots \tilde{\mathbf{B}}_e^{b^m} \dots] \quad \forall m \in \mathcal{N}_t^e \quad (60)$$

The contribution of the l th branch function of each tip m to the element matrix $\tilde{\mathbf{B}}_e^b$ is denoted $\tilde{\mathbf{B}}_e^{b^m}$ and is as follows:

$$\tilde{\mathbf{B}}_e^{b^m} |_{l=1,2,3,4} = \begin{bmatrix} \mathcal{B}_{1K}^{b^m} & 0 & \dots \\ 0 & \mathcal{B}_{2K}^{b^m} & \dots \\ \mathcal{B}_{2K}^{b^m} & \mathcal{B}_{1K}^{b^m} & \dots \end{bmatrix} \quad \forall K \in \mathcal{K}_e^m \text{ and } \forall m \in \mathcal{N}_t^e \quad (61)$$

The terms $\mathcal{B}_{1K}^{b^m}$ and $\mathcal{B}_{2K}^{b^m}$ are:

$$\mathcal{B}_{1K}^{b^m} = \frac{\partial(\tilde{N}_K(\mathbf{x})\tilde{F}_{lK}^m(\mathbf{x}))}{\partial x} \frac{\partial \Pi_x^j}{\partial x} + \frac{\partial(\tilde{N}_K(\mathbf{x})\tilde{F}_{lK}^m(\mathbf{x}))}{\partial y} \frac{\partial \Pi_y^j}{\partial x} \quad (62)$$

$$\mathcal{B}_{2K}^{b^m} = \frac{\partial(\tilde{N}_K(\mathbf{x})\tilde{F}_{lK}^m(\mathbf{x}))}{\partial x} \frac{\partial \Pi_x^j}{\partial y} + \frac{\partial(\tilde{N}_K(\mathbf{x})\tilde{F}_{lK}^m(\mathbf{x}))}{\partial y} \frac{\partial \Pi_y^j}{\partial y} \quad (63)$$

After construction of the virtual force vector $\tilde{\mathbf{f}}_{\Pi_j}$, the virtual displacement field $\tilde{\mathbf{d}}_j$ needed for the computation of the derivative of the energy release rate $\partial G_i / \partial \ell_j$ is obtained by:

$$\tilde{\mathbf{d}}_j = \mathbf{K}^{-1} \tilde{\mathbf{f}}_{\Pi_j} \quad (64)$$

where $\tilde{\mathbf{d}}_j$ is the global virtual displacement created by a virtual unit displacement Π_j of tip j and is defined at all nodes of the cell. Equation (64) needs to be solved for each tip j . Therefore, a vector field $\tilde{\mathbf{F}}_{\Pi_j}$ needs to be constructed for each tip j , and a displacement vector $\tilde{\mathbf{d}}_j$ is solved for each tip j . The matrix \mathbf{K} is the stiffness matrix of the system defined in Section 3.

The derivative of the energy release rate at tip i with respect to tip j is computed by:

$$\frac{\partial G_i}{\partial \ell_j} = \tilde{\mathbf{d}}^T \left(\int_{\Omega} (\tilde{\mathbf{B}}^T \mathbf{C} \tilde{\mathbf{B}}_{\Theta_i} + \tilde{\mathbf{B}}_{\Theta_i}^T \mathbf{C} \tilde{\mathbf{B}} - \tilde{\mathbf{B}}^T \mathbf{C} \tilde{\mathbf{B}}) d\Omega \right) \tilde{\mathbf{d}}_j^T = \tilde{\mathbf{d}}^T \tilde{\mathbf{K}}_{\Theta_i} \tilde{\mathbf{d}}_j^T \quad (65)$$

The matrix $\tilde{\mathbf{B}}_{\Theta_i}$ is constructed in the same manner as $\tilde{\mathbf{B}}_{\Pi_j}$, with the function Θ_i instead of Π_j . Θ_i is defined at tip i and has a non-zero gradient on an annular region of smaller average radius r_i (2.4 times the length of an element). $\bar{\mathbf{d}}$ is the generalized displacement defined in Equation (30). The structure of the virtual displacement $\tilde{\mathbf{d}}_j$ is identical to the structure of the generalized displacement $\bar{\mathbf{d}}$ in Equation (30).

A matrix $[\partial G_i / \partial \ell_j]$ is constructed for the competitive cracks $\mathcal{N}_{\text{comp}}$ at time step t_{n-1} . All subdeterminants of this matrix are computed. The maximum subdeterminant gives the set of tips \mathcal{N}_{act} that will grow at time step t_n determined by:

$$\begin{aligned} \mathcal{N}_{\text{act}} &= \left\{ i \in \mathcal{N}_{\text{comp}} \middle/ \max_{\{i,j\} \in \mathcal{N}_{\text{comp}}} \det \left(-\frac{\partial^2 \mathcal{L}(\ell, \mathbf{u})}{\partial \ell_i \partial \ell_j} \right) \right. \\ &= \left. \max_{\{i,j\} \in \mathcal{N}_{\text{comp}}} \det \left(\frac{\partial(G_i(\sigma_o) - G_c^i)}{\partial \ell_j} \right) \geq 0 \right\} \end{aligned} \quad (66)$$

The subdeterminant of the derivatives of the energy release rate with the highest value, when positive, corresponds to the path that causes the most damage to the structure with the least energy; the crack configuration is unstable; in that case the crack can grow without any change of loading. When the maximum subdeterminant is negative, the crack configuration is stable. In this case we choose the configuration that dissipates the least energy. This configuration is the one that gives the smallest rising slope in the global load deflection response, the steepest softening slope or the most drastic snap-back. The fracture equilibrium state is said to be critical when the subdeterminant is zero [50]. Each active crack is grown by an increment given by Equation (44).

4.4. Flowchart

The flowchart of the multiple crack growth algorithm is:

***At time step t_1 ,** the structure is precracked, and we compute the load parameter λ to bring at least one crack to K_c and perform the stability analysis to determine the cracks that will grow at time step t_2 .

***For each time step t_n , $n > 1$:**

- **Step 1:** add the crack increment computed by Equation (44) in the direction of the maximum hoop stress according to Equation (21) to the active tips \mathcal{N}_{act} determined at time step t_{n-1} . Tests are performed to detect any free boundary touching or crack junctions.

- **Step 2:** Obtain the displacements $\bar{\mathbf{d}}$ by Equation (33) for the traction \mathbf{t}_o and $\lambda = 1$. Compute the stress intensity factors K_{eq}^i with the interaction integral and the local critical stress intensity factor K_c^i at each tip for inhomogeneous material. Determine the tip β with the stress intensity factor $K_{\text{eq}}^\beta(\sigma_o)$ the closest to the critical value K_c^β (Equation (45)) and compute the load parameter λ (Equation (46)). We compute the traction $\mathbf{t} = \lambda \mathbf{t}_o$ that should be applied to the structure to respect Equation (14) and the corresponding displacement $\bar{\mathbf{u}}$. A set of competitive cracks $\mathcal{N}_{\text{comp}}$ is established (Equation (11)).

- **Step 3:** A stability analysis is performed for the set of cracks $\mathcal{N}_{\text{comp}}$ by Equation (66). The maximum subdeterminant of the matrix of the derivatives of the energy release rate of the

set of cracks $\mathcal{N}_{\text{comp}}$ provides the subset of crack tips \mathcal{N}_{act} that are grown at time step t_{n+1} . (When the maximum subdeterminant is positive \mathcal{N}_{act} is obtained directly, when negative one should look for the crack combinations among all possible combinations of subsets in $\mathcal{N}_{\text{comp}}$ yielding the minimum dissipation). Return to step 1.

5. RESULTS

The method is applied in several examples to study the accuracy of the stress intensity factors and the derivative of the energy release rate, the junction representation and the stability analysis by comparison to previous solutions. The model is also applied to problems with a random distribution of cracks.

In all examples, we consider a material with properties similar to a weak glass with a Young's modulus of 10^5 psi and Poisson's ratio of 0.3, the critical stress intensity factor $K_c = 800$ psi in^{1/2}. All examples are in plane strain. In all examples we consider a unit thickness and isothermal conditions.

In the unit cell problems, in each step n , the displacement of the edges \bar{u} is computed by averaging the displacements of the nodes of the edge loaded under the traction \mathbf{t} . The displacement \bar{u} and the nominal traction $\|\mathbf{t}\|$ are used to characterize the overall response of the body. In all of the examples, we report nominal strain and nominal stress given by:

$$\varepsilon^{\text{nom}} = \frac{\bar{u}}{H} \quad (67a)$$

$$\sigma^{\text{nom}} = \|\mathbf{t}\| \quad (67b)$$

where H is the height of the sample.

5.1. Accuracy of the derivative of the energy release rate

We consider an edge crack of initial length 0.30 in in a plate as shown in Figure 8. The plate is more than three times longer than wide to make possible a comparison with the analytic solution in an infinite strip by Tada [51]. The plate is subjected to a traction $\mathbf{t}_o = \sigma_o \mathbf{n}$ at its top and bottom edges. The bottom left node is fixed and the displacement in y of the bottom right node is constrained to vanish. The mesh is unstructured and is finer around the crack. It contains 870 elements and 1797 nodes. The material is homogeneous, so G_c is constant in the entire body.

An analytical solution for this problem can be found in Reference [51] for crack lengths $\ell \leq 0.6 W$, where W is the width. The stress intensity factor for a crack of length ℓ is:

$$K = \frac{\sigma_o \sqrt{2W \tan(\pi\ell/2W)}}{\cos(\pi\ell/2W)} \left(0.752 + 2.02 \frac{\ell}{W} + 0.37 \left(1 - \sin \frac{\pi\ell}{2W} \right)^3 \right) \quad (68)$$

The analytical expression for the derivative of the energy release rate [51] is:

$$\frac{\partial G}{\partial \ell} = \frac{2K}{E'} \frac{\partial K}{\partial \ell} \quad (69)$$

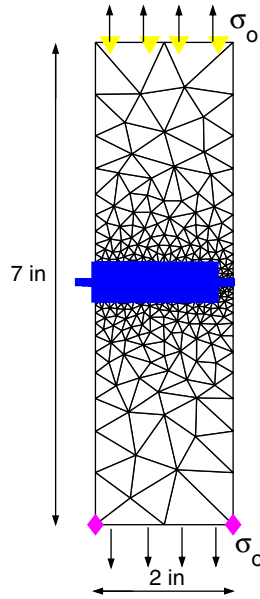


Figure 8. Mesh for edge crack in a plate problem.

The numerical stress intensity factor can be computed either by the J -integral (16) or from the stress intensity factors K_I and K_{II} by (19).

Figure 9(a) shows the nominal stress versus the nominal strain. It can be seen that after a linear response to the point where the crack reaches the critical stress intensity factor K_c , the crack starts to grow and snapback occurs. Figure 9(b) and (c) show a slight divergence for the longest crack length; at that length, Tada's formula is not valid anymore. Table I gives the stress intensity factors obtained by (16) or (19) and the derivative of the energy release rate. The normalized error is at most 0.5% for the stress intensity factors and at most 2% for the derivative of the energy release rate. The snapback branch can be captured only if the loading process is controlled by a monotonically increasing function; in this case the crack length was used.

5.2. Junction problem

To test the modelling of a junction between two cracks, we consider two cracks in a square plate of width 2 in. The plate is subjected to a traction $\sigma_o = 10^3$ psi, at its top edge. The bottom left node is fixed and the displacement in the y direction of all the bottom nodes vanish. The mesh is unstructured and consists of 5228 elements and 10 653 nodes. The total crack length increment $\Delta\ell_m$ is 0.06 in. There is no analytical solution for this problem. Figure 10(a) shows the initial cracks and Figure 10(b) the final crack configuration.

Several observations are employed to define the discretization for this problem and the other examples. First, this method is more accurate when the crack length increment $\Delta\ell_m$ is between half and twice the element size. Second, the coalescence algorithm described in Section 3 is more reliable when the initial cracks are discretized into segments approximately the size of

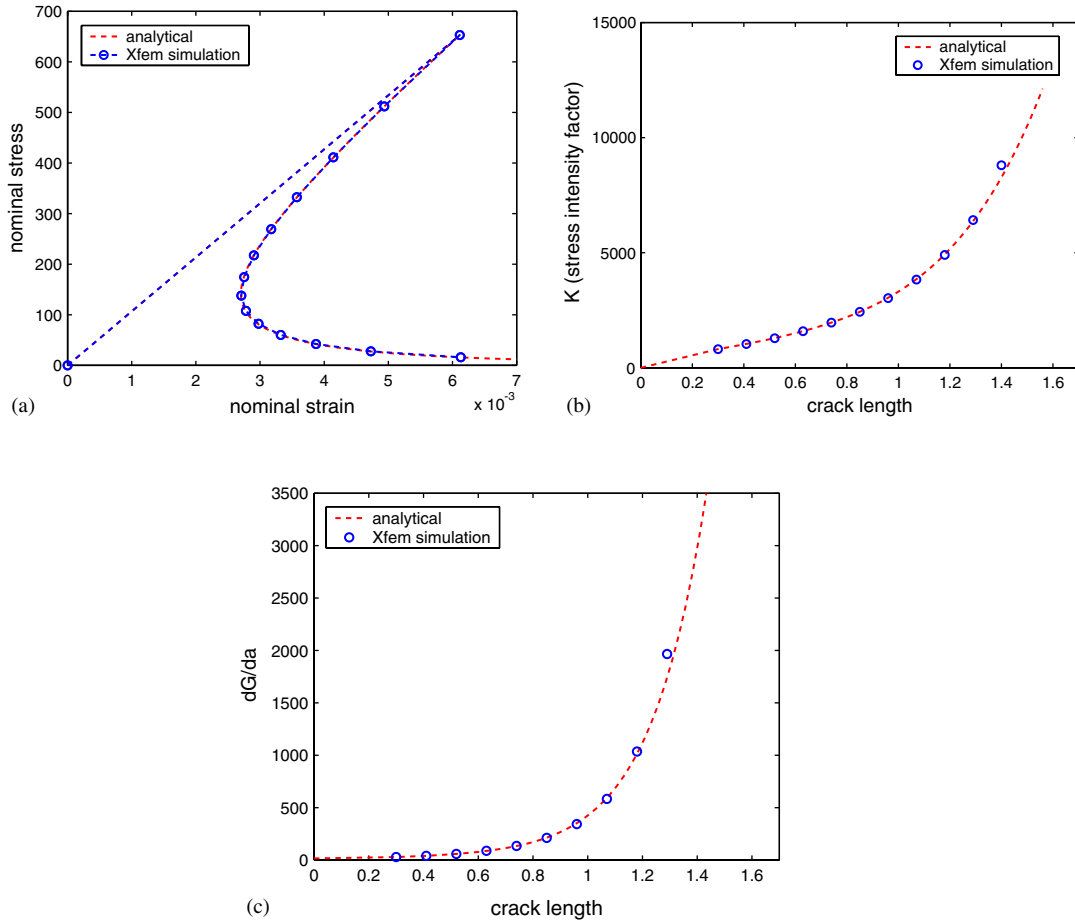


Figure 9. Numerical results for edge cracked plate compared to analytical results of Tada *et al.* [51]: (a) load deflection curve; (b) stress intensity factor (equivalent) in $\text{psi in}^{1/2}$, the crack length is in inches; and (c) derivative of the energy release rate in lb in^{-1} .

Table I. Comparison of numerical and analytical values of the mode I stress intensity factor (K_I) and the derivative of the energy release rate for an edge crack in an infinite strip.

Crack length		0.30	0.41	0.52	0.63	0.74	0.85	0.96
K^{analy} ($\text{psi in}^{1/2}$)	$1.0\text{e}03 \times$	0.8104	1.0356	1.2908	1.5918	1.9605	2.4283	3.0385
$K_{\text{eq}}^{\text{xfem}}$ ($\text{psi in}^{1/2}$)	$1.0\text{e}03 \times$	0.8084	1.0312	1.2839	1.5884	1.9610	2.4282	3.0268
Relative error in K (%)		0.24	0.42	0.54	0.21	-0.026	0.0023	0.39
$K_{(J\text{-integ})}$ ($\text{psi in}^{1/2}$)	$1.0\text{e}03 \times$	0.8078	1.0310	1.2835	1.5883	1.9610	2.4289	3.0289
$(dG/da)^{\text{analy}}$ (psi)	$1.0\text{e}3 \times$	0.0288	0.0408	0.0588	0.0870	0.1337	0.2132	0.3514
$(dG/da)^{\text{xfem}}$ (psi)	$1.0\text{e}3 \times$	0.0282	0.0403	0.0587	0.0880	0.1349	0.2119	0.3436
Relative error in dG/da (%)		2.05	1.34	0.16	-1.11	-0.90	0.61	2.22

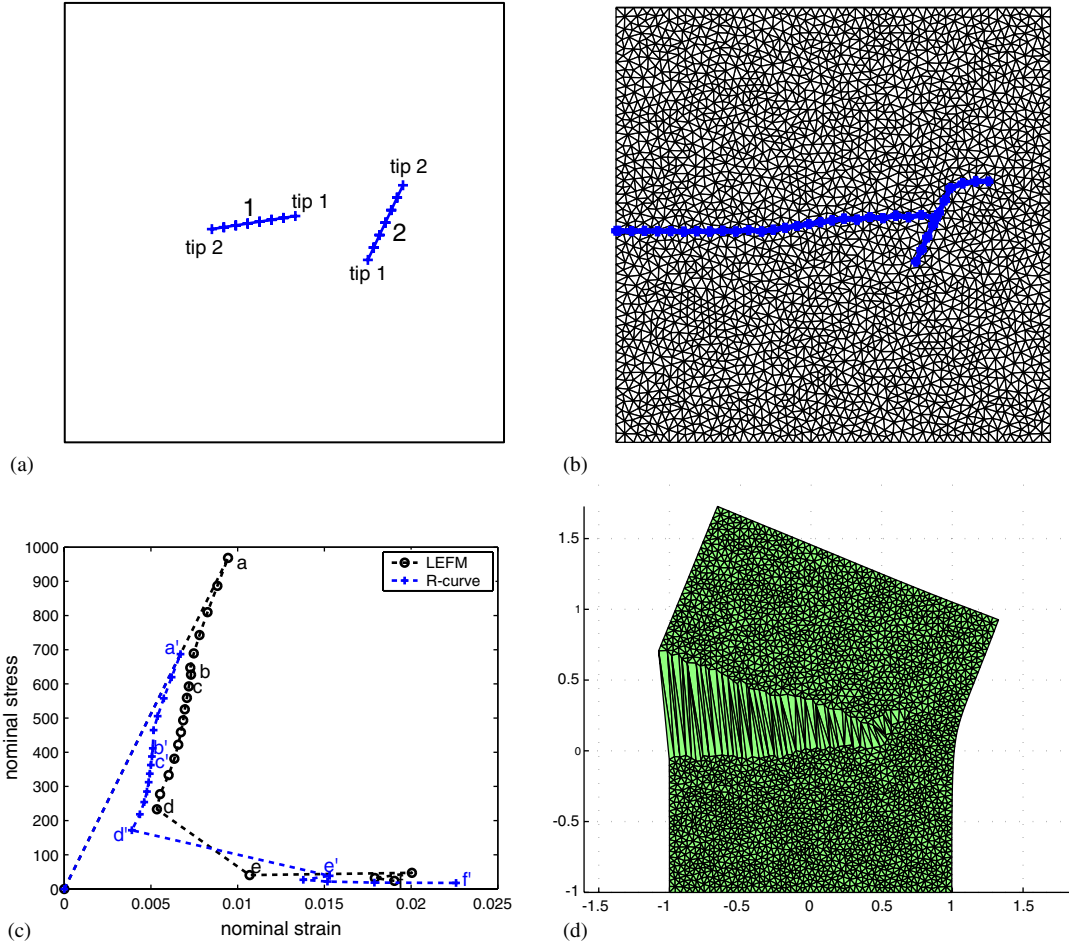


Figure 10. (a) Mesh of a unit cell containing two cracks (initial cracks); (b) final configuration; (c) load deflection curve of the plate (plane strain) for the Linear Elastic Fracture Mechanic (LEFM) and R -curve problem; and (d) deformed mesh (displacement multiplied by a factor 2×10^5).

the crack length increment. Third, the J -integral gives the most accurate stress intensity factors when the domain of integration of one tip does not contain another tip. The initial cracks should thus span at least 5 elements. Bellec and Dolbow [52] have given an enrichment for shorter cracks but this was not used here. Therefore the procedure to set a mesh is as follows. First the lengths of the initial cracks determine the choice of the element size. In this example, the length of crack 1 is 0.3847 in (centre-point $(-0.14, 0)$ with angle 9°) and the length of crack 2 is 0.3858 in (centre-point $(0.46, 0)$ with angle 64.8°), the element size is taken as 0.04 in. Then the crack length increment is set between half and twice the element size, here $\Delta \ell_m = 0.06$ in. Finally, the initial cracks are discretized by segments of length about the size of $\Delta \ell_m$, here the initial crack 1 is discretized by 7 segments of length 0.055 in, and crack 2 in 6 segments of length 0.0626 in, see Figure 10(a).

Figure 10(d) shows that the plate opening after the two cracks have coalesced. This opening was made possible by the junction expression described in Equation (23). Figure 10(c) shows the applied nominal stress as a function of the nominal strain. The curve with circles represents the behaviour of a brittle homogeneous material where G_c is constant in the body. The curve with crosses represents the behaviour of a material in which the crack growth law is described by an R -curve:

$$G_c^i = G_c(1 - \exp(-k\Delta\ell_i)) \quad (70)$$

where k is the R -curve parameter of the material.

As shown in Figure 10(c), the load increases linearly until point a as no crack growth occurs. From point a to b , tip 1 of crack 1 grows to the right and connects to crack 2. During this phase, the load must be decreased and the displacement of the loaded surface must also be decreased; i.e. snapback occurs. From point c to point e , tip 2 of crack 1 grows to the left and connects the edge of the plate. At point d , crack 1 still has both tips inside the plate, but at point e , tip 2 of crack 1 has reached the edge of the plate. From point d to point e , the problem switches from a plate with only interior cracks to a plate with a dominant edge crack. The path between d and e releases substantial energy in connecting the crack to the edge of the plate. After point e , tip 2 of crack 2 grows to the right until point f in Figure 10(c).

The material described with an R -curve approach exhibits similar behaviour with lower strength. As in the previous results, substantial work is dissipated from d' to e' , when tip 2 of crack 1 connect the edge of the plate. When we refine the mesh, the paths of the cracks and the load deflection curve converge.

5.3. Multiple crack tip problem

To test the stability algorithm developed in Section 4, we considered a centre-cracked panel where the two tips initially have identical stress intensity factors. The material is homogeneous with G_c constant. The plate has a width of 2in and a height of 7in. The crack length increment is 0.06in; the mesh contains 1468 elements and 3005 nodes. The applied traction σ_o is 781 psi. The analytical solution for the diagonal terms of the matrix of the derivatives of the energy release rate in the initial configuration is $0.1210 \times 10^2 \text{ psi in}^{1/2}$. (Note that the derivative of the energy release rate for the full plate and centre crack has an analytical solution half of the value given in Reference [51].) The value given in Tada is for half of the plate and symmetric boundary conditions.) Our finite element model gives $0.1231 \times 10^2 \text{ psi in}^{1/2}$.

According to Bazant and Cedolin [50], when both tips grow simultaneously, the path is unstable (case 1 in Figure 11(a)), while, when only one tip grows, the growth is stable (case 2). The latter crack path dissipates the least amount of energy and should be observed first until the crack tip reaches the side of the plate (case 2) and then the edge crack should grow until percolation (case 3). Our algorithm computes the same evolution. The load deflection curve is shown in Figure 11(b) and compared to an analytical solution constructed from Reference [51]; it first follows a stable crack path (case 2) from point a to c , which is steeper than the unstable crack path (case 1), and then the edge crack grows (case 3), from point c to d .

We note that the determinant of the matrix of the derivatives of the energy release rate $[\partial G_i / \partial \ell_j]$ is nearly zero and corresponds to case 1 in Figure 11(a). Therefore any point in this pathway is a bifurcation point [50]. Because of small numerical differences between the tips of

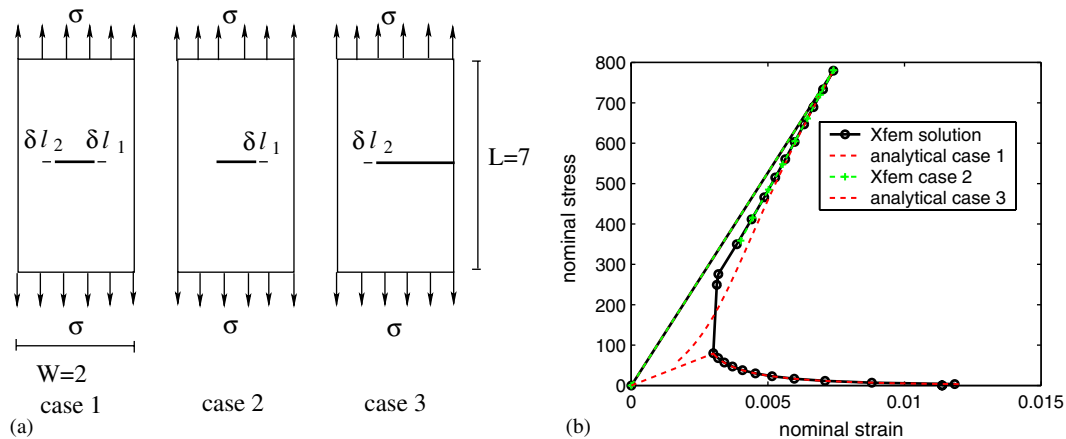


Figure 11. (a) Possible paths of centre-cracked panel; and (b) load deflection curve of the plate with a centre crack (plane strain). The circles markers on a solid line are for our solution with the stability analysis algorithm.

the crack due to the asymmetry of the mesh, the algorithm detects a maximum subdeterminant in the matrix of derivatives of the energy release rate, resulting in the growth of only one tip. (If the mesh were perfectly symmetric, we would have two maximum subdeterminants for each tip, and we could randomly choose one of them.)

In Figure 11(b), we join the last point of the first branch following case 2 with the first point of the second branch following case 3. We do so because the amount of energy released during the percolation of the last small ligament of material is unknown. This type of approximation can also be found in Reference [31].

5.4. Random distribution of cracks

We consider a square of width 2 in containing 10 initial cracks shown in Figure 12(a). The cell is loaded by tension at the top and bottom edges with the displacement on the bottom right and left corner nodes prescribed to zero in the y direction ($u_{yA} = u_{yB} = 0$). The displacement of the bottom left corner node in the x direction is prescribed equal to zero ($u_{xA} = 0$). The material properties are that of a glass given previously. The mesh contains 5228 elements and 10 653 nodes. The average element size is 0.04 in and the crack increment is 0.07 in.

The force–deflection curve, expressed as a nominal stress versus nominal strain curve, is shown in Figure 12(b). It exhibits snapback and is similar to the response of a cell percolated by a single crack; the growth sequence is given in Table II.

Figures 13(b) and (d) show the responses of the same cell for two heterogeneous materials, denoted material 1 and 2. In the heterogeneous material, the critical stress intensity factor is a function of the spatial co-ordinates and given by:

$$G_c(x, y) = G_c \left[1 + C_A \left[\sin \frac{x}{w_x} + \sin \frac{y}{w_y} \right] \right] \quad (71)$$

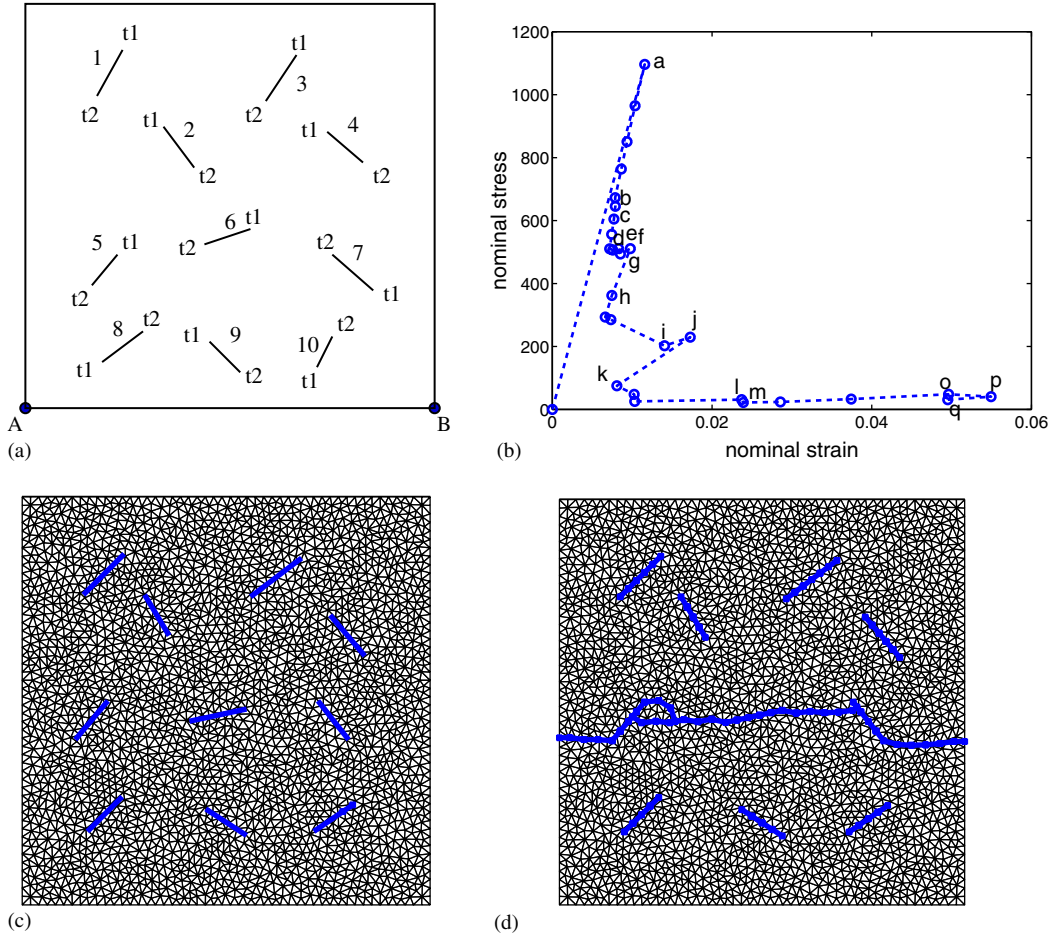


Figure 12. (a) Schematic of plate; (b) load deflection curve of the cell after 28 steps just before percolation (the work of separation = 6.26 lbs in); (c) mesh of a homogeneous unit cell containing ten cracks (initial configuration); and (d) final configuration.

with:

$$w_x = \frac{W}{\pi n_x}, \quad w_y = \frac{H}{\pi n_y} \tag{72}$$

where W is the width of the plate and H is the height. For heterogeneous material 1, $C_A = 0.43$ and $n_x = n_y = 10$, and for heterogeneous material 2, $C_A = 0.45$ and $n_x = n_y = 8$.

The inhomogeneity of the materials changes the paths of the cracks and the order in which the cracks grow compared to the homogeneous material. Furthermore, the load-deflection behaviour becomes more complex with the initial drop in the load followed by an increase as the dominant crack tip enters tougher material. An interesting feature of the inhomogeneous model is that the nominal stress decreases less rapidly than for the homogeneous model even though the

Table II. Sequence of crack growth in the homogeneous material.

Load deflection	Crack growth sequences
From <i>a</i> to <i>b</i>	Crack 6 tip 2 grows to the left
From <i>c</i> to <i>d</i>	Crack 6 tip 1 grows to the right
From <i>e</i> to <i>f</i>	Crack 6 tip 2 grows and connects to crack 5
Point <i>g</i>	Crack 6 tip 1 grows
From <i>h</i> to <i>i</i>	Crack 5 tip 2 grows to the left and connects the edge of the plate
Point <i>j</i>	Crack 6 tip 1 connects to crack 7
Point <i>k</i>	Crack 6 tip 1 joins crack 7
From <i>l</i> to <i>m</i>	Crack 5 tip 1 grows and dies, cannot connect 6 again
From <i>n</i> to <i>o</i>	Crack 7 tip 1 grows to the right
Point <i>p</i>	Crack 7 tip 2 dies, cannot connect 6 again
After point <i>q</i>	Crack 7 tip 1 grows to the right and connect to edge of the plate

mean strength of the two models is equivalent, i.e. there is less snapback. However, the overall work of separation is about the same.

Another example of the capabilities of the crack growth algorithm is shown Figure 14. In this example, the cracks are grown by a Paris-type law which ensures the growth of many cracks in each step (see Reference [53]). When the procedure to set a discretization described previously is respected, the crack paths are almost mesh independent. These paths resemble experimental results for specimens containing random multiple cracks [13]. Examples of fatigue crack growth problems can be found in Reference [54].

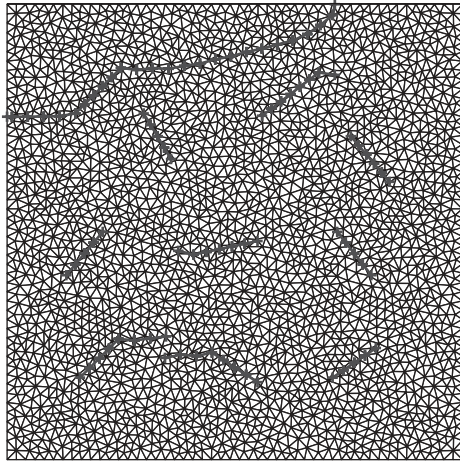
6. CONCLUSIONS

The extended finite element method has been applied to problems of multiple crack growth. The method seems particularly suitable for multiple crack growth because remeshing is avoided.

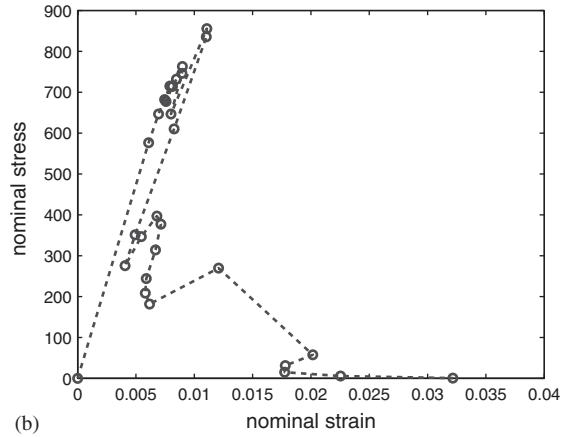
The choice of higher order elements which are quadratic for the standard displacement field and linear for the enrichment gives an accurate crack solution. In contrast to boundary element methods, it can easily handle inhomogeneous materials and internal features, such as grain boundaries.

Our algorithm models static crack growth. The cracks to be grown are chosen explicitly based on the information at the end of the previous step. However at each timestep, the point of the load deflection curve is obtained that satisfies exactly both equilibrium (13) and the brittle crack growth law (14). The energy release rate of the crack β in (45) is equal to the critical value.

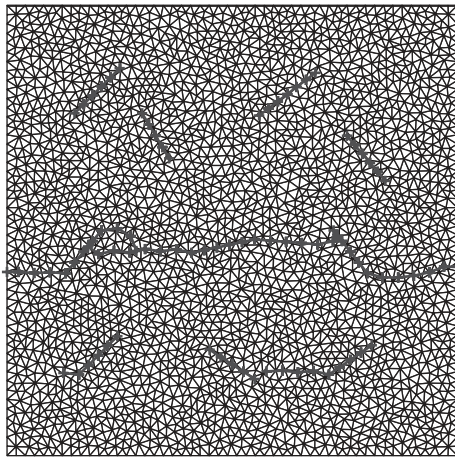
The presence of multiple cracks requires the modelling of cracks penetrating edges and crack interaction conditions. A representation of junctions between two cracks was implemented in here. The algorithm allows cracks to connect in the growth process. The simulation can thus be run until complete failure of the solid. The procedures for joining cracks reaching a free boundary are somewhat heuristic and arbitrary. Some improvement could be obtained by using smaller steps before these events occur. However the gaps in the force-deflection curves due to these heuristics are quite small.



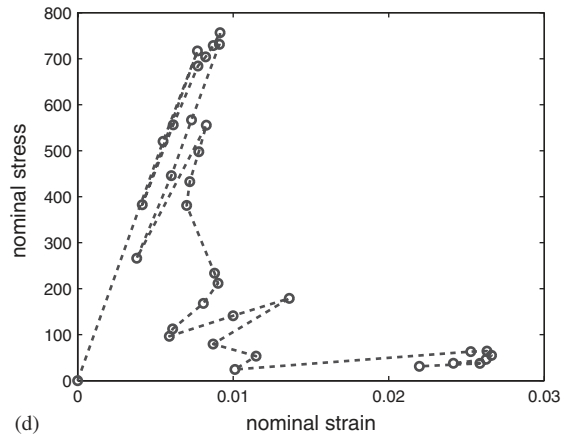
(a)



(b)



(c)



(d)

Figure 13. (a) Final configuration (heterogeneous material 1); (b) load deflection curve of the cell with heterogeneous medium after 28 steps by X-FEM simulation before percolation (heterogeneous material 1) (plane strain) (the work of separation = 6.69 lbs in); (c) final configuration (heterogeneous material 2); and (d) load deflection curve of the cell with heterogeneous medium after 33 steps by X-FEM simulation before percolation (heterogeneous material 2) (plane strain) (the work of separation = 6.16 lbs in).

A stability analysis for crack growth was introduced in a linear elastic fracture mechanics context. The stability analysis is based on the derivative of the energy release rate. The expression for the derivative of the energy release rate developed by Suo and Combescure [47, 48] and Suo and Valeta [49], has been adapted to the X-FEM formulation. This enables the method to rationally select the cracks that are growing in the given time step.

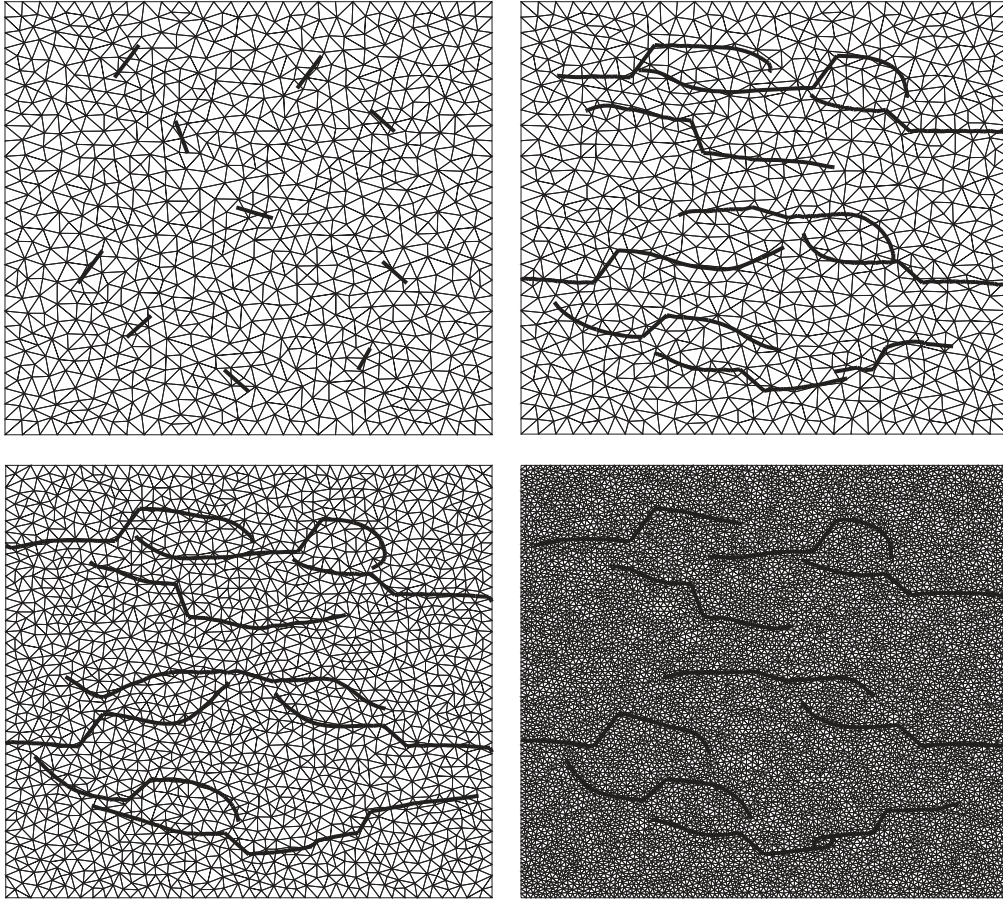


Figure 14. Initial and final configurations of 10 cracks in a unit-cell under tension until percolation. Three different meshes are shown: $h^{ave} = 0.07$ cm top left (initial configuration); $h^{ave} = 0.07$ cm top right (final configuration); $h^{ave} = 0.05$ cm bottom left (final configuration); $h^{ave} = 0.02$ cm bottom right (final configuration), where h^{ave} is an average element size; the cell is square with a width of 2 cm [53].

The results show good agreement with analytic solutions for stress intensity factors, the derivative of the energy release rate, and the junction of cracks. The overall response of the structure matches analytic solutions. We considered multiple crack models with as many as ten cracks, but the model can support an arbitrary number of cracks.

ACKNOWLEDGEMENTS

The authors are grateful for the research support Office of Naval Research and Department of Energy. We are also grateful to Giulio Ventura for his comments and suggestions.

REFERENCES

1. Belytschko T, Black T. Elastic crack growth in finite elements with minimal remeshing. *International Journal for Numerical Methods in Engineering* 1999; **45**(5):601–620.
2. Belytschko T, Moës N, Usui S, Parimi C. Arbitrary discontinuities in finite elements. *International Journal for Numerical Methods in Engineering* 2001; **50**(4):993–1013.
3. Melenk JM, Babuska I. The partition of unity finite element method: basic theory and applications. *Computer Methods in Applied Mechanics and Engineering* 1996; **39**:289–314.
4. Dolbow J, Moës N, Belytschko T. An extended finite element method for modeling crack growth with frictional contact. *Computer Methods in Applied Mechanics and Engineering* 2001; **190**(51–52):6825–6846.
5. Moës N, Dolbow J, Belytschko T. A finite element method for crack growth without remeshing. *International Journal for Numerical Methods in Engineering* 1999; **46**(1):131–150.
6. Osher S, Sethian JA. Fronts propagating with curvature dependent speed: algorithms based on Hamilton–Jacobi formulations. *Journal of Computational Physics* 1998; **79**(1):12–49.
7. Sethian JA. *Level Sets Methods & Fast Marching Methods: Evolving Interfaces in Computational Geometry, Fluid Mechanics, Computer Vision and Materials Science*. Cambridge University Press: Cambridge, UK, 1999.
8. Burchard P, Cheng LT, Merriman B, Osher S. Motion of curves in three spacial dimensions using a level set approach. *Journal of Computational Physics* 2001; **170**:720–741.
9. Osher S, Cheng LT, Kang M, Shim Y, Tsai YH. Geometric optics in a phase-space-based level set and Eulerian framework. *Journal of Computational Physics* 2002; **179**(2):622–648.
10. Ventura G, Xu JX, Belytschko T. A vector level set method and new discontinuity approximations for crack growth by EFG. *International Journal For Numerical Methods in Engineering* 2002; **54**:923–944.
11. Ventura G, Budyn E, Belytschko T. Vector level sets for description of propagating cracks in finite elements. *International Journal of Numerical Methods in Engineering* 2003; **58**:1571–1592.
12. Tanaka K, Akiniwa Y, Shimizu K. Propagation and closure of small cracks in SiC particulate reinforced aluminum alloy in high cycle and low cycle fatigue. *Engineering Fracture Mechanics* 1996; **55**(5):751–762.
13. Lawler J. Hybrid fiber-reinforcement in mortar and concrete. *Ph.D. Thesis*, Department of Civil and Environmental Engineering, Northwestern University, December 2001.
14. Barpi F, Valente S. Size-effects bifurcation phenomena during multiple cohesive crack propagation. *International Journal of Solids and Structures* 1998; **35**(16):1851–1861.
15. Datsyshin AP, Savruk MP. A system of arbitrarily oriented cracks in elastic solids. *Journal of Applied Mathematics and Mechanics* (PMM, translation of the Russian Journal ‘Prikladnaya Matematika i Mekhanika’) 1973; **37**(2):306–332.
16. Kachanov M. Elastic solids with many cracks: a simple method of analysis. *International Journal of Solids and Structures* 1987; **23**(1):23–43.
17. Kachanov M. A simple technique of stress analysis in elastic solids with many cracks. *International Journal of Fracture* 1985; **28**:R11–R19.
18. Kachanov M. Macrocrack interaction. *International Journal of Fracture* 1986; **30**:R65–R72.
19. Rubinstein A. Macrocrack interaction with semi-infinite microcrack array. *International Journal of Fracture* 1985; **27**:113–119.
20. Rubinstein A. Macrocrack–Microdefect interaction. *Journal of Applied Mechanics* 1996; **53**:505–510.
21. Rubinstein A. Crackpath effect on material toughness. *Journal of Applied Mechanics* 1990; **57**:97–103.
22. Freij-Ayoub R, Dyskin AV, Galybin AN. The dislocation approximation for calculating crack interaction. *International Journal of Fracture* 1997; **86**:L57–L62.
23. Chen YZ. General case of multiple cracks problems in an infinite plate. *Engineering Fracture Mechanics* 1984; **20**(4):591–597.
24. Bolotin VV. Reliability against fatigue fracture in presence of sets of cracks. *Engineering Fracture Mechanics* 1996; **53**(5):753–759.
25. Yang JN, Manning SD. A simple second order approximation for stochastic crack growth analysis. *Engineering Fracture Mechanics* 1996; **53**(5):677–686.
26. Lua YJ, Liu WK, Belytschko T. A stochastic damage model for the rupture prediction of a multi-phase solid, Part II: Statistical approach. *International Journal of Fracture* 1992; **55**:341–361.
27. Liu WK, Chen Y, Belytschko T, Lua YJ. Three reliability methods for fatigue crack growth. *Engineering Fracture Mechanics* 1996; **33**(5):733–752.

28. Lua YJ, Liu WK, Belytschko T. Elastic interactions of a fatigue crack with a micro-defect by the mixed boundary integral equation method. *International Journal for Numerical Methods in Engineering* 1993; **36**: 2743–2759.
29. McDowell DI. An engineering model for propagation of small cracks in fatigue. *Engineering Fracture Mechanics* 1997; **56**(3):357–377.
30. Rybaczuk M, Stoppel P. The fractal growth of fatigue defects in materials. *International Journal of Fracture* 2000; **103**:71–94.
31. Carpinteri A, Monetto I. Snap-back analysis of fracture evolution in multi-cracked solids using boundary element method. *International Journal of Fracture* 1990; **98**:225–241.
32. Moran B, Shih CF. A general treatment of crack tip contour integrals. *International Journal of Fracture* 1987; **35**:295–310.
33. Yau J, Wang S, Corten H. A mixed-mode crack analysis of isotropic solids using conservation laws of elasticity. *Journal of Applied Mechanics* 1980; **47**:335–341.
34. Bazant ZP, Planas J. *Fracture and Size Effect in Concrete and Other Quasi-brittle Materials*. CRC Press: Boca Raton, London, 1998.
35. Stazi FL, Budyn E, Chessa J, Belytschko T. An extended finite element method with higher-order elements for curved cracks. *Computational Mechanics* 2002; **31**:38–48.
36. Chessa J, Wang HW, Belytschko T. On construction of blending elements for local partition of unity enriched finite elements. *International Journal for Numerical Methods in Engineering* 2003; **57**:1015–1038.
37. Fleming M, Chu YA, Moran B, Belytschko T. Enriched element-free Galerkin methods for singular fields. *International Journal for Numerical Methods in Engineering* 1997; **40**(8):1483–1504.
38. Kienzler R, Herrmann G. Fracture criteria based on local properties of the Eshelby tensor. *Mechanics Research Communications* 2002; **29**(6):521–527.
39. Bolander JE Jr., Saito S. Fracture analysis using spring networks with random geometry. *Engineering Fracture Mechanics* 1998; **61**:569–591.
40. Demir I, Zbib HM, Khaleel M. Microscopic analysis of crack propagation for multiple cracks, inclusions and voids. *Theoretical and Applied Fracture Mechanics* 2001; **36**:147–164.
41. Deng H, Nemat-Nasser S. Microcrack arrays in isotropic solids. *Mechanics of Materials* 1992; **13**:15–36.
42. Nemat-Nasser S, Hori M. Toughening by partial or full bridging of cracks in ceramics and fiber reinforced composites. *Mechanics of Materials* 1987; **6**:245–269.
43. Daux C, Moës N, Dolbow J, Sukumar N, Belytschko T. Arbitrary branched and intersecting cracks with the extended finite element methods. *International Journal for Numerical Methods in Engineering* 2000; **48**: 1741–1760.
44. Bocca T, Carpinteri A, Valente S. Mixed mode fracture of concrete. *International Journal of Solids and Structures* 1991; **27**:1139–1153.
45. Nguyen QS, Stolz C. Endomagement, fatigue, rupture—Sur le problème en vitesse de propagation de fissure et de déplacement en rupture fragile ou ductile. Note de Nguyen Quoc Son et Claude Stolz, présentée par Paul Germain. *Comptes-Rendus de l'Académie des Sciences de Paris* 1985; **301**(Série II)(10):661–664.
46. Nguyen QS, Stolz C, Debruyne G. Energy methods in fracture mechanics: stability, bifurcation and second variations. *European Journal of Mechanics – A/Solids* 1990; **2**:157–173.
47. Suo XZ, Combesure A. Sur une formulation mathématique de la dérivée seconde de l'énergie potentielle en théorie de la rupture fragile. *Comptes-Rendus de l'Académie des Sciences de Paris* 1989; **308**(Série II): 1119–1122.
48. Suo XZ, Combesure A. Double virtual crack extension method for crack growth stability assessment. *International Journal of Fracture* 1992; **57**:127–150.
49. Suo XZ, Valeta MP. Second variation of energy and an associated line independent integral in fracture mechanics. II Numerical validations. *European Journal of Mechanics – A/Solids* 1998; **17**(4):541–565.
50. Bazant ZP, Cedolin L. *Stability of Structures*. Oxford University Press: New York, Oxford, 1991.
51. Tada H, Paris PC, Irwin GR. *The Stress Analysis of Cracks Handbook*. Del Research Corporation: Hellerton, PA, 1973.
52. Bellec J, Dolbow JE. A note on enrichment functions for modelling crack nucleation. *Communications in Numerical Methods in Engineering* 2003; **19**:921–932.
53. Budyn E. Multiple crack growth by the extended finite element method. *Ph.D. Thesis*, Department of Mechanical Engineering, Northwestern University, June 2004.
54. Stolarska M, Chopp DL. Modeling thermal fatigue cracking in integrated circuits by level sets and the extended finite element method. *International Journal of Engineering Science* 2003; **41**:2381–2410.